Available online at www.sciencedirect.com
SCIENCE DIRECT
Journal of Catalysis 229 (2005) 265–275
JOURNAL OF CATALYSIS
www.elsevier.com/locate/jcat

Trends in low-temperature water–gas shift reactivity on transition metals

N. Schumacher [a,*], A. Boisen [a,b], S. Dahl [b], A.A. Gokhale [c], S. Kandoi [c], L.C. Grabow [c], J.A. Dumesic [c], M. Mavrikakis [c], I. Chorkendorff [a]

[a] *Interdisciplinary Research Center for Catalysis (ICAT), Department of Physics and Department of Chemical Engineering, Technical University of Denmark, Building 312, DK-2800 Kgs. Lyngby, Denmark*
[b] *Haldor Topsøe A/S, Nymøllevej 55, DK-2800 Kgs. Lyngby, Denmark*
[c] *Department of Chemical and Biological Engineering, University of Wisconsin-Madison, Madison, WI 53706, USA*

Received 11 August 2004; revised 25 October 2004; accepted 25 October 2004

Available online 23 December 2004

Abstract

Low-temperature water–gas shift reactivity trends on transition metals were investigated with the use of a microkinetic model based on a redox mechanism. It is established that the adsorption energies for carbon monoxide and oxygen can describe to a large extent changes in the remaining activation and adsorption energies through linear correlations. In comparisons with experimental data it is found that the model predicts well the order of catalytic activities for transition metals, although it fails to quantitatively describe the experimental data. This discrepancy could be due to the assumption that the redox mechanism dominates and to the neglect of adsorbate interactions, which play an important role at high coverages. The model predicts that the activity of copper can be improved by increasing the strengths with which carbon monoxide and oxygen are bonded to the surface, thus suggesting possible directions for improving the catalyst for low-temperature WGSR.
© 2004 Elsevier Inc. All rights reserved.

Keywords: Water–gas shift; Microkinetic model; Transition metals; Activity; Turnover frequency

1. Introduction

The WGS reaction

$$H_2O(g) + CO(g) \rightleftarrows H_2(g) + CO_2(g)$$

is an important component of several industrial processes. It is primarily used to produce high-purity hydrogen, for example, for ammonia synthesis. Because the reaction is moderately exothermic, low temperature favors a high equilibrium conversion of CO. In industrial applications the reaction is run at pressures around 25–35 bar. To achieve the highest feasible conversion, two adiabatic stages with cooling in between are needed [1]: a high temperature shift at 310–450 °C with a catalyst based on iron oxide structurally promoted with chromium oxide, followed by a low temperature shift in the temperature range of 210–240 °C, where the typical industrial catalyst is copper with zinc oxide and aluminum oxide as support materials. The copper catalyst undergoes deactivation at temperatures higher than 300 °C, as the copper particles sinter because of surface migration [2].

The WGS and its reverse reaction are also an integral part of methanol synthesis, where methanol is synthesized from a mixture of CO, CO_2, and H_2, with CO_2 hydrogenation being the major path [3]. Here the WGS reaction is much faster and must be taken into the equilibrium considerations for the overall reaction [4].

In recent years there has been renewed interest in the WGS reaction in connection with fuel cell-powered vehicles, where hydrogen is obtained via partial oxidation and steam reforming of hydrocarbons. The reformed fuel contains 1–10% CO [5], which, apart from being a pollutant, also poisons the Pt anode in the fuel cell, because of its strong adsorption to the electrode surface [6]. The lowering of the CO

* Corresponding author. Fax: +45 45 93 23 99.
E-mail address: nana.schumacher@fysik.dtu.dk (N. Schumacher).

0021-9517/$ – see front matter © 2004 Elsevier Inc. All rights reserved.
doi:10.1016/j.jcat.2004.10.025

content is limited by equilibrium at the operating temperature of the conventional $Cu/ZnO/Al_2O_3$ WGS catalyst in the reformer system. The development of a more active catalyst would allow one to lower the temperature and reduce the volume of the reformer system. Inspired by recent work with modeling and optimization of the ammonia synthesis catalyst [7,8], we developed a microkinetic model for WGS over copper catalysts to describe the WGS reaction over other transition metals. This approach allows us to suggest how the low-temperature WGS catalyst may be improved. We note here that our model only treats metallic Cu, whereas Cu^+ has also been suggested as a possible active site [9]. We have found the evidence for metallic copper overwhelming and have therefore used the approach presented here.

2. Theory and modeling

The WGS reaction has previously been studied extensively by Campbell et al. [10–12] and modeled by Ovesen et al. [13–16] on Cu surfaces and industrial Cu catalysts for the low-temperature shift with the use of the so-called surface redox mechanism [12]. In the following analysis we shall rely on this mechanism, but the method presented here can easily accommodate future alternative mechanisms that may prove more relevant for more metals/catalysts. In this respect, our approach addresses the performance of an optimal WGS catalyst operating by the redox mechanism. The same methodology can then be implemented elsewhere as information about alternative WGS reaction mechanisms becomes available. Based on the redox model, we investigate whether it is possible to describe the WGS activity of transition metals in general. In principle, this is done by assuming that the reaction mechanism is the same for all metals. Then only the vibrational frequencies and the adsorption energies[1] of the surface intermediates, as well as the activation energies of the rate-determining steps, must be changed. However, based on previous experience with the ammonia synthesis reaction, we have decided to neglect the changes in vibrational frequencies [17]; that is, we are assuming that the vibrations are the same as they are on Cu.

The adsorption energies for the adsorbed species are calculated from periodic, self-consistent density functional theory (DFT) calculations [18], whereas the activation energies are estimated from Brøndsted–Evans–Polanyi (BEP) relations [19]. Two sets of chemisorption energies were used: one from Nørskov and co-workers [19] calculated with the RPBE functional for chemisorption of species on step sites, and one from Mavrikakis and co-workers[2] calculated with PW91 for chemisorption of species on close-packed surface terraces. In general, steps bind species stronger than do terraces, whereas PW91 overestimates binding compared with RPBE. As a result, it should be acceptable to compare results based on the two data sets.

The following redox mechanism is used as the basis of the kinetic model:

1. $H_2O(g) + * \rightleftarrows H_2O^*$;
2. $H_2O^* + * \rightarrow H^* + OH^*$ (RCS);
3. $2OH^* \rightleftarrows H_2O^* + O^*$;
4. $OH^* + * \rightarrow O^* + H^*$ (RCS);
5. $2H^* \rightleftarrows H_2(g) + 2^*$;
6. $CO(g) + * \rightleftarrows CO^*$;
7. $CO^* + O^* \rightarrow CO_2^* + *$ (RCS);
8. $CO_2^* \rightleftarrows CO_2(g) + *$;
9. $H^* + CO_2^* \rightleftarrows HCOO^* + *$.

Here * represents a surface site consisting of two copper atoms, and elementary reaction steps 2, 4, and 7 are assumed to be rate-controlling steps (RCS). The theory needed for the kinetic model has previously been published by Ovesen et al. [13,14]. In this study the set of parameters for the copper surface is a revised version taken from Ovesen et al. [16].

3. Estimating energy trends

To extend the microkinetic model to describe the WGS activity of other transition metals besides Cu, it is necessary to establish how the activation energies of the three rate-controlling steps and the adsorption energies for the seven adsorbed species are affected by the catalyst, that is, a total of ten parameters.

We assume that the activation energies are related via the reaction energies through the Brøndsted–Evans–Polanyi relation. For an activated reaction the BEP relation involves a linear dependence between the activation energy, E_a, and the reaction energy, E_r [19,20]. Because our concern here is the changes in the activation energy, ΔE_a, we encounter when switching to a metal other than Cu, we will use the BEP relation in the following form:

$$\Delta E_a = \alpha \, \Delta E_r, \tag{1}$$

where α is the BEP correlation constant. Nørskov and coworkers [20] found that for the dissociation of N_2, CO, NO, and O_2 on close-packed surfaces, $\alpha = 0.90 \pm 0.04$, and for steps sites on these surfaces, $\alpha = 0.87 \pm 0.05$. For simplicity we assume a common value of $\alpha = 0.9$ for a reaction where bonds not involving hydrogen are broken. Equivalently, the correlation factor is 0.1 when such bonds are formed (elementary reaction step 7) (see Fig. 1). The value $\alpha = 0.65$ estimated by Pallassana et al. [21] is used for reactions where bonds containing hydrogen are broken (elementary reaction steps 2 and 4). The reaction energies for the rate-controlling steps are obtained from the calculated chemisorption energies.

[1] The correct term is "ground-state energies" [13,14], but this is not critical, as the relative change from one metal to another will be equivalent for ground-state and adsorption energies.

[2] A.A. Gokhale, S. Kandoi, L.C. Grabow, J.A. Dumesic, M. Mavrikakis, unpublished observations.

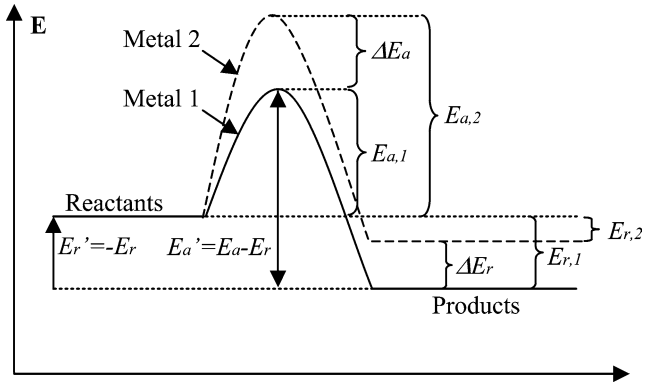

Fig. 1. Energy diagram for an activated reaction on two different metals, 1 and 2. $E_{a,1}$ and $E_{a,2}$ are the activation energies on the respective metals, and ΔE_a is the difference. The same nomenclature is used for the reaction energy E_r. Energies marked with ($'$) are for the reverse reaction. From the figure it can easily be deduced that if $\Delta E_a = \alpha\,\Delta E_r$ then $\Delta E'_a = (1-\alpha)\Delta E'_r$.

Trends in the adsorption energies of the seven adsorbed species can be estimated from data for chemisorption energies on the metals in question. The molecular and dissociative chemisorption energies are obtained from DFT calculations. In particular, the adsorption energies for H_2O and CO_2 are assumed to be constant on all metals considered, since these molecules do not interact strongly with the metal surfaces. In support of this simplification, we note here that H_2O desorbs at 150 K [22] and CO_2 desorbs at 90 K [23], as measured from typical TPD experiments, clearly indicating physisorption. This assumption reduces the number of variable parameters in the general model to eight in total. Furthermore, the number of independent parameters can be reduced even further, since some of these eight variable parameters are found to correlate linearly.

Chemisorption energies for HCOO, H_2O, and CO_2 are not available from the original set of data from Nørskov and co-workers. The HCOO RPBE data were supplied by Mavrikakis and co-workers. Fig. 2a shows the linear correlation between the reaction energies of the three rate-controlling steps and the chemisorption energy for oxygen, and Figs. 2b and c show the correlation between the chemisorption energies for OH, H, CO, CO_2, H_2O, and HCOO and the chemisorption energy for oxygen. Fig. 3 shows the corresponding correlations with the chemisorption energy for CO. From these figures it is clear that all of the energies correlate linearly with the chemisorption energy of either oxygen or CO. This behavior is illustrated in Tables 1 and 2, which show the deviation s from the linear fits, where s is given as

$$s = \sqrt{\frac{\sum_i (y_i - y_{r,i})^2}{n}}, \tag{2}$$

y_i is a value from the data set, $y_{r,i}$ is the corresponding value from the regression, and n is the number of values in the data set.

Table 1
The table shows the deviation of the data from the linear fits, s, for chemisorption and reaction energies vs chemisorption energies of the two species, CO and O for the remaining eight parameters

	E_{CO}	E_O
$E_{r,2}$ ($H_2O^* + * \rightarrow OH^* + H^*$)	0.567	**0.194**
$E_{r,4}$ ($OH^* + * \rightarrow O^* + H^*$)	0.535	**0.223**
$E_{r,7}$ ($CO^* + O^* \rightarrow CO_2^* + *$)	0.991	**0.479**
E_{CO} ($CO(g) + * \rightleftarrows CO^*$)	**0**	0.478
E_{OH} ($OH(g) + * \rightleftarrows OH^*$)	0.529	**0.107**
E_H ($\frac{1}{2}H_2(g) + * \rightleftarrows H^*$)	**0.080**	0.184
E_O ($\frac{1}{2}O_2(g) + * \rightleftarrows O^*$)	0.992	**0**
E_{HCOO} ($HCOO(g) + * \rightleftarrows HCOO^*$)	0.314[a]	**0.164**[a]

Notice that the deviation factor for CO and oxygen naturally is zero. The bold values are the best correlations for E_{CO} and E_O. Chemisorption energies from [19] for adsorption on step sites were used.
[a] Values have been calculated using unpublished RPBE data on closed pocked surfaces supplied by Mavrikakis and co-workers.

Table 2
Comparison of deviation from the linear fits, s, of chemisorption and reaction energies vs chemisorption energies for CO and O as shown in Table 1, but now using binding energies from Mavrikakis and co-workers for adsorption on terrace sites

	E_{CO}	E_O
$E_{r,2}$ ($H_2O^* + * \rightarrow OH^* + H^*$)	0.446	**0.139**
$E_{r,4}$ ($OH^* + * \rightarrow O^* + H^*$)	**0.215**	0.322
$E_{r,7}$ ($CO^* + O^* \rightarrow CO_2^* + *$)	0.540	**0.446**
E_{CO} ($CO(g) + * \rightleftarrows CO^*$)	**0**	0.450
E_{OH} ($OH(g) + * \rightleftarrows OH^*$)	0.407	**0.174**
E_H ($\frac{1}{2}H_2(g) + * \rightleftarrows H^*$)	**0.081**	0.172
E_O ($\frac{1}{2}O_2(g) + * \rightleftarrows O^*$)	0.550	**0**
E_{HCOO} ($HCOO(g) + * \rightleftarrows HCOO^*$)	0.304	**0.146**
E_{CO_2} ($CO_2(g) + * \rightleftarrows CO_2^*$)	0.057	**0.055**
E_{H_2O} ($H_2O(g) + * \rightleftarrows H_2O^*$)	**0.092**	0.101

The bold values mark the best correlations for E_{CO} and E_O.

Thus, when the chemisorption energies found by Nørskov and co-workers [19] are used, it is possible to reduce the number of parameters we need to vary to study trends in WGS from eight to two, namely the changes in O and CO binding energies, ΔE_O and ΔE_{CO}, respectively. The following correlations are needed for this purpose:

$$\begin{aligned}
\Delta E_{r,2} &= 0.66 \cdot \Delta E_O, & \Delta E_{r,4} &= 0.64 \cdot \Delta E_O,\\
\Delta E_{r,7} &= -1.31 \cdot \Delta E_O, & \Delta E_{OH} &= 0.51 \cdot \Delta E_O,\\
\Delta E_{HCOO} &= 0.43 \cdot \Delta E_O, & \Delta E_H &= 0.41 \cdot \Delta E_{CO}.
\end{aligned} \tag{3}$$

The Brøndsted–Evans–Polanyi relation is then used to estimate the activation energies:

$$\begin{aligned}
\Delta E_{a,2} &= 0.65 \cdot 0.66 \cdot \Delta E_O, & \Delta E_{a,4} &= 0.65 \cdot 0.64 \cdot \Delta E_O,\\
\Delta E_{a,7} &= -0.1 \cdot 1.31 \cdot \Delta E_O.
\end{aligned} \tag{4}$$

Nearly the same correlations are found for the data set from Mavrikakis and co-workers, except for the correlation of the activation energy for reaction step 4, $E_{r,4}$, where the

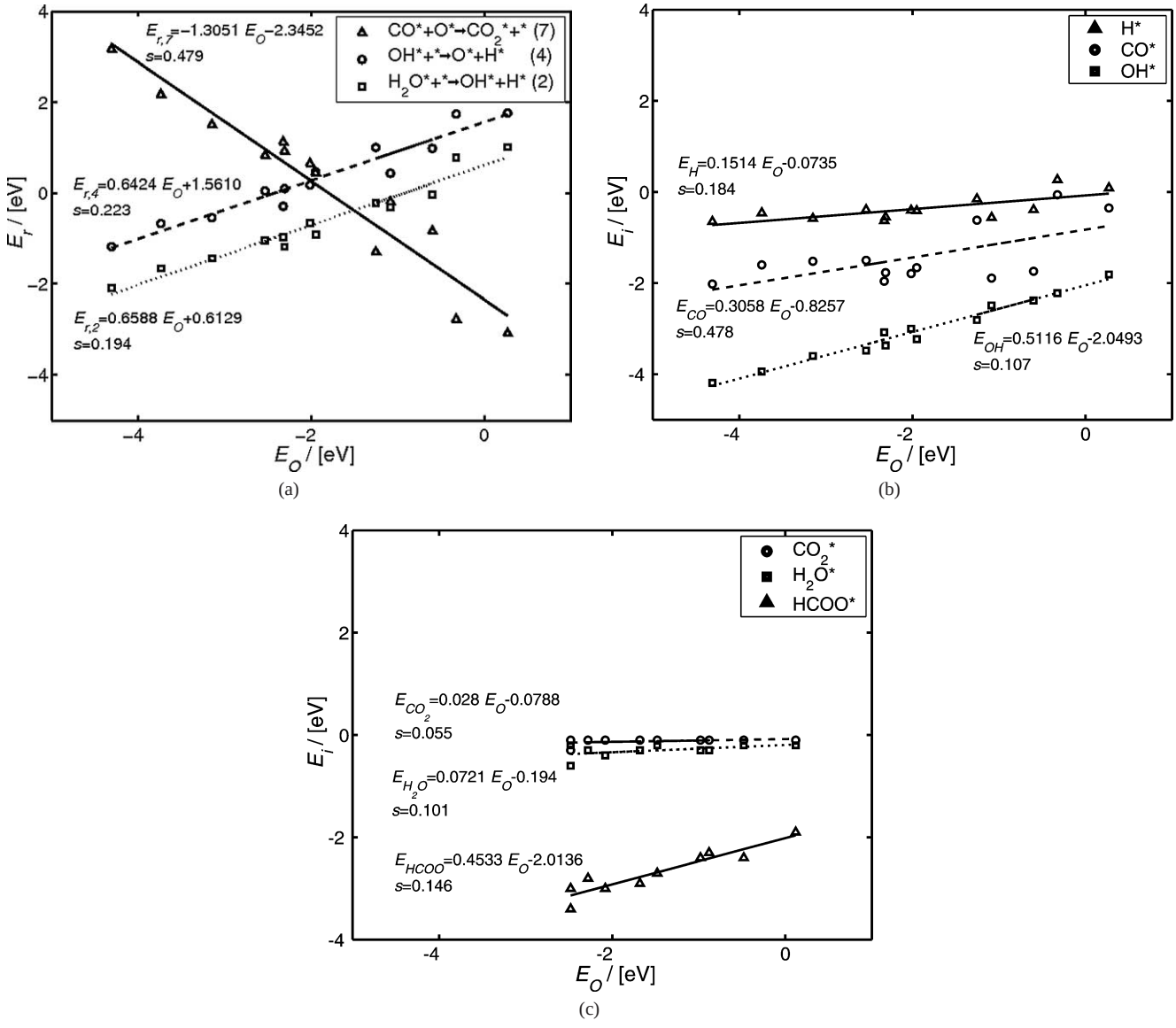

Fig. 2. (a) The linear correlation between the chemisorption energy for oxygen, E_O, and the reaction energies, E_r, of the rate determining steps. (b) The correlation between the chemisorption energy for oxygen and the energies for OH, H, and CO. (a) and (b) are from [19]. (c) Correlations for HCOO, CO_2, and H_2O, PW91 data from Mavrikakis and co-workers.

linear correlation is slightly better with the chemisorption energy of carbon monoxide than with the chemisorption energy of atomic oxygen. However, for reasons of comparison we decided to use the chemisorption energy for oxygen. Table 2 shows the deviation from the linear fits for the data set from Mavrikakis and co-workers. In this set of data, the chemisorption energies for CO_2 and H_2O are given, but the slopes are insignificant compared with the other correlations (see Figs. 2 and 3). Therefore they are again assumed to be constant.

Using the chemisorption energies from Mavrikakis and co-workers calculated with PW91 for chemisorption on terraces, we derived the following linear correlations, thereby reducing the number of free variable parameters to two:

$$\Delta E_{r,2} = 0.72 \cdot \Delta E_O, \qquad \Delta E_{r,4} = 0.76 \cdot \Delta E_O,$$
$$\Delta E_{r,7} = -1.59 \cdot \Delta E_O, \qquad \Delta E_{OH} = 0.52 \cdot \Delta E_O,$$
$$\Delta E_{HCOO} = 0.45 \cdot \Delta E_O, \qquad \Delta E_H = 0.41 \cdot \Delta E_{CO}. \tag{5}$$

And the activation energies are

$$\Delta E_{a,2} = 0.72 \cdot 0.67 \cdot \Delta E_O, \qquad \Delta E_{a,4} = 0.76 \cdot 0.78 \cdot \Delta E_O,$$
$$\Delta E_{a,7} = -0.1 \cdot 1.59 \cdot \Delta E_O \tag{6}$$

4. Results and discussion

We are now able to describe the WGS rate over transition metal surfaces as a function of the binding energies of atomic oxygen and of CO. Fig. 4 shows the three-dimensional volcano plot based on chemisorption energies on step sites from

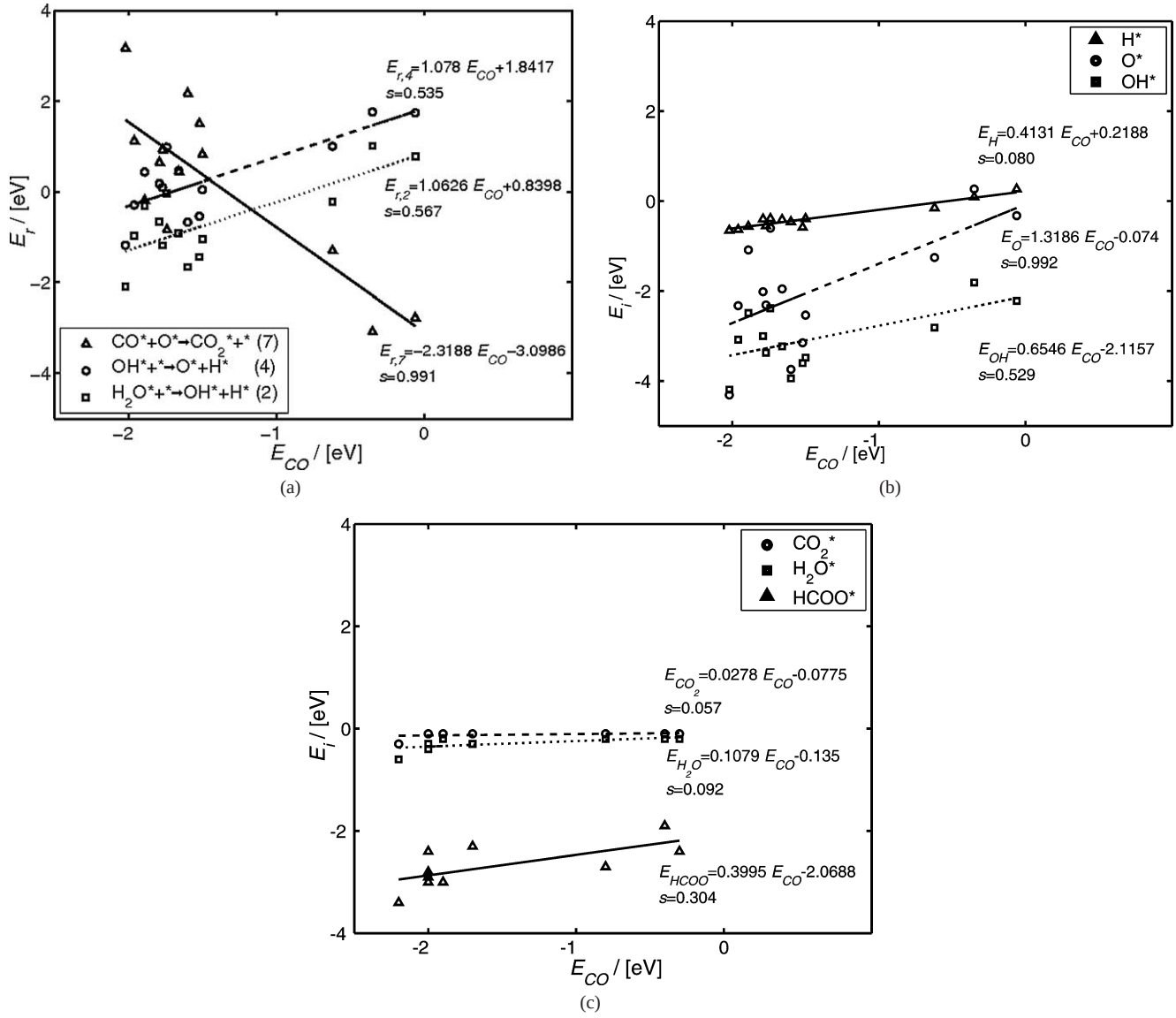

Fig. 3. (a) The linear correlation between the chemisorption energy for carbon monoxide, E_{CO}, and the reaction energies, E_r, of the rate determining steps. (b) The correlation between the chemisorption energy for carbon monoxide and the energies for OH, H, and CO. (a) and (b) are from [19]. (c) Correlations for HCOO, CO_2, and H_2O, PW91 data from Mavrikakis and co-workers.

Nørskov and co-workers [19], and Fig. 5 shows a close-up of the area around the maximum turnover frequency (TOF). Note that the chemisorption energies for all metals are given relative to the copper values (negative ΔE means stronger adsorption than on Cu). An extra set of coordinates, $(E_O, E_{CO}) = (-0.35\text{ eV}, -0.5\text{ eV})$, has been added for Au_{10} nanoparticles [24].

From the model, one can understand why this volcano appears by analyzing the most abundant reaction intermediates (MARI) on the surface. This prediction is illustrated in Fig. 6. The variation in surface coverage of the reaction intermediates is again illustrated when the adsorption energies of CO and O are changed relative to Cu. It can be seen that CO is the predominant surface intermediate at ΔE_{CO} below 0 eV. However, when ΔE_O becomes lower than −1 eV, oxygen begins to dominate the surface. Hydroxyl (OH) species are abundant when $\Delta E_O \in [-1; 0]$ eV, and $\Delta E_{CO} \in [-0.5; 1]$ eV. In the same parameter region, formate (HCOO) is present at the surface. Considerable coverage of surface hydrogen (H) is present when ΔE_O ranges from 0 to 2 eV, and $\Delta E_{CO} = 0$ eV. H_2O and CO_2 are present on the surface only when all other coverages are low and free sites are available. On the various metals, it is observed that Fe, Mo, and W are almost entirely covered with O, whereas Ni, Rh, Ru, Ir, Pd, and Pt are covered with CO. Cu, Au_{10}, Au, and Ag present only small coverages of both of these species.

Figs. 7 and 8 show the turnover frequencies obtained when the model is based on data from Mavrikakis and co-workers for chemisorption on terrace sites. It should be noted that the monometallic surfaces have different coordinates $(\Delta E_O, \Delta E_{CO})$ compared with Figs. 4 and 5. The variation

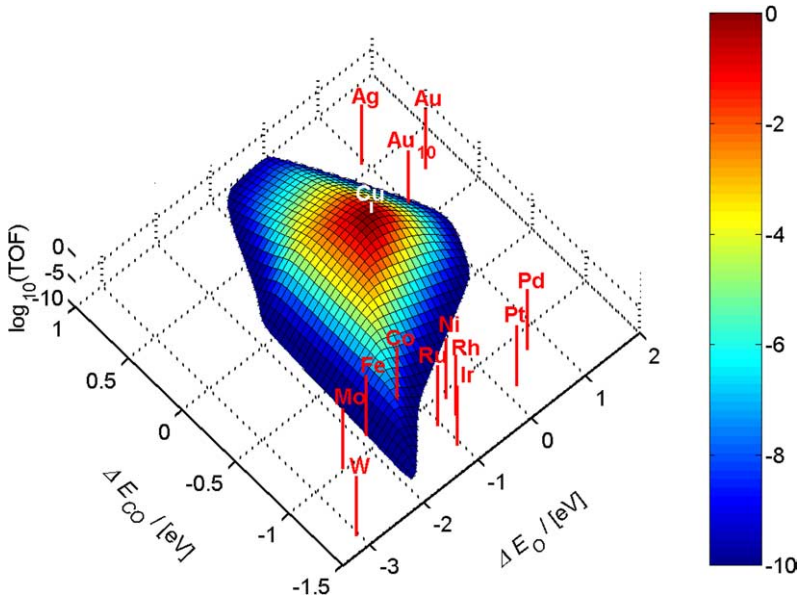

Fig. 4. The turnover frequency of the WGS reaction at varying adsorption energies of carbon monoxide and oxygen is illustrated. Extent of reaction $\xi = 0$, $p = 30$ bar, $T = 225\,^{\circ}\mathrm{C}$, and the feed gas composition is 2.5% CO, 12.5% CO_2, 37.5% H_2, 25%, H_2O, and balance N_2. The three-dimensional volcano plot is based on chemisorption energies from Nørskov and co-workers [19]. The chemisorption energies for all metals are given relative to the copper values.

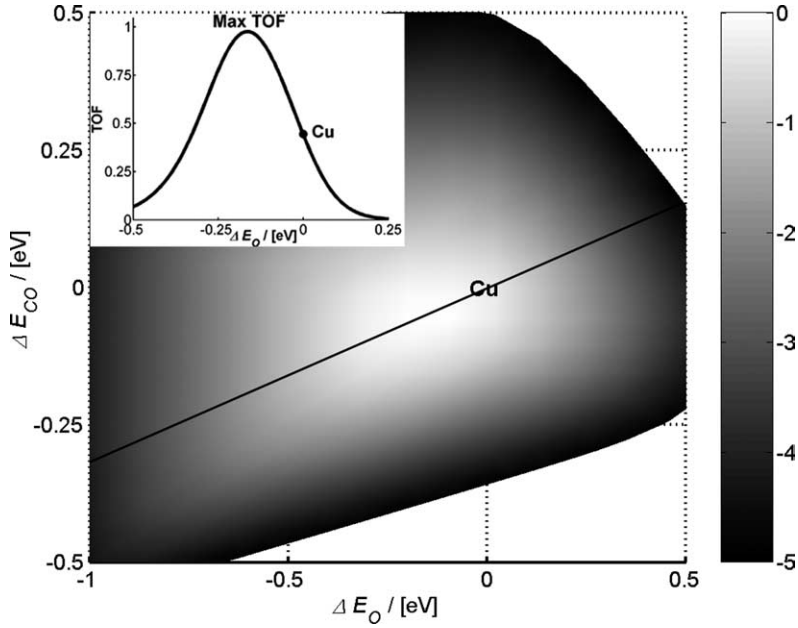

Fig. 5. A close up of the maximum turnover frequency (TOF) at $\xi = 0$, $p = 30$ bar, $T = 225\,^{\circ}\mathrm{C}$, and a feed gas composition of 2.5% CO, 12.5% CO_2, 37.5% H_2, 25%, H_2O, and balance N_2. Based on chemisorption energies from Nørskov and co-workers [19]. Insert displays a cut through the maximal TOF and the TOF for Cu.

in surface coverages is not shown, since it is similar to the results based on the data of Nørskov and co-workers. Again it is seen that the Cu coordinates are close to the coordinates for the maximum TOF, and the optimal WGS catalyst is a metal that binds O and CO slightly more strongly than Cu (see Fig. 8). At the limit of zero conversion ($\xi = 0$), the maximum TOF is estimated to be slightly higher for the data of Mavrikakis and co-workers ($\mathrm{TOF_{max}} = 1.0\ \mathrm{s^{-1}}$) than for the data of Nørskov and co-workers ($\mathrm{TOF_{max}} = 0.97\ \mathrm{s^{-1}}$).

The position of the maximum of the volcano plot is sensitive to reaction conditions. As a result, the optimal catalyst is not the same as the reaction proceeds and CO and H_2O are converted. Fig. 9 shows that as conversion increases in passing through the reactor, the optimal catalyst changes to one that binds CO more strongly and O more weakly. The concept of an optimal catalyst curve has previously been introduced for ammonia synthesis [8]. Fig. 10 illustrates how increasing pressure results in movement of the maximum

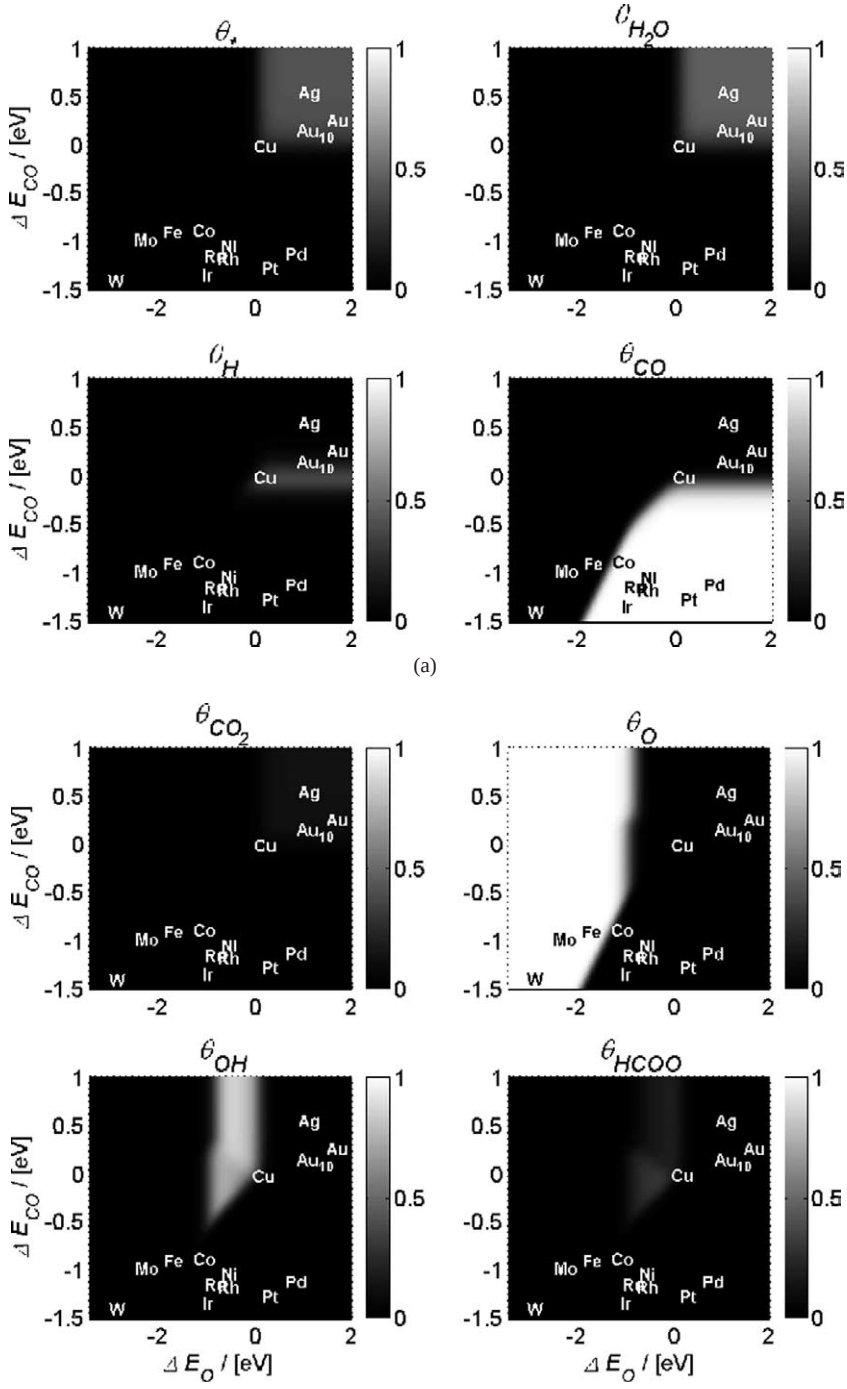

Fig. 6. Surface coverage of the reaction intermediates at varying adsorption energies of carbon monoxide and oxygen relative to Cu (negative ΔE means more reactive than Cu). $\xi = 0$ at $p = 30$ bar, $T = 225\,^{\circ}\mathrm{C}$, and the feed gas composition is 2.5% CO, 12.5% CO_2, 37.5% H_2, 25%, H_2O, and balance N_2. Chemisorption energies from Nørskov and co-workers [19] for adsorption on step sites are used.

turnover frequency toward higher ΔE_{CO} and ΔE_O, that is, towards weaker adsorption. At high pressure (20–40 bar) the predominant effect on the optimal TOF is caused by changing ΔE_{CO}, which may imply that at the position of the maximal TOF the CO coverage is high compared with that of oxygen. This behavior corresponds well with the findings in Fig. 6 for 30 bar. Increasing the temperature (see Fig. 11) produces an effect that is the opposite of that produced by increasing the pressure. The reduction in coverage now has to be compensated for by a change in ΔE_{CO}. Again it is seen that the coverage of carbon monoxide is higher than that of oxygen in the region in question, and the effect of changing ΔE_O is small. These results are similar for the two data sets.

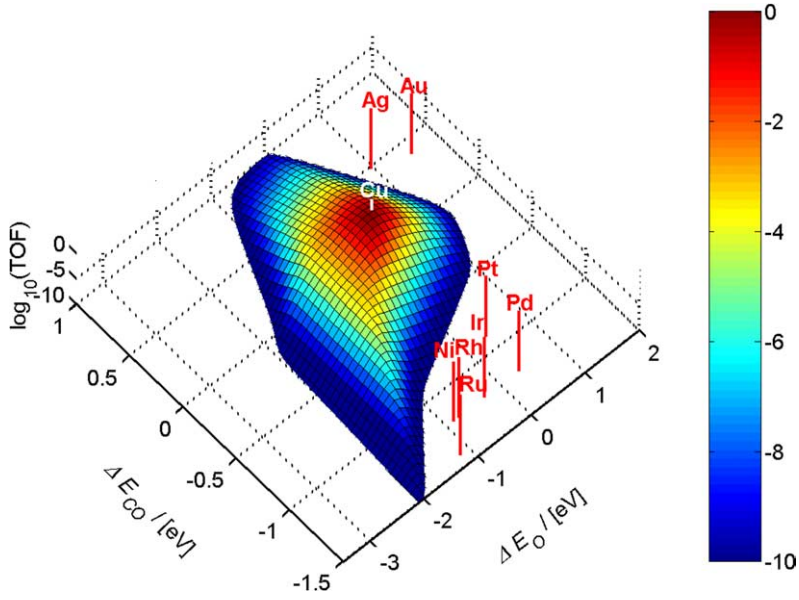

Fig. 7. The turnover frequency of the WGS reaction at varying adsorption energies of carbon monoxide and oxygen is illustrated. Extent of reaction $\xi = 0$, $p = 30$ bar, $T = 225\,^{\circ}\mathrm{C}$, and the feed gas composition is 2.5% CO, 12.5% CO_2, 37.5% H_2, 25%, H_2O, and balance N_2. The two-dimensional volcano plot is based on chemisorption energies from Mavrikakis and co-workers for chemisorption on terrace sites. It should be noted that the metal coordinates are different compared to Figs. 4 and 5.

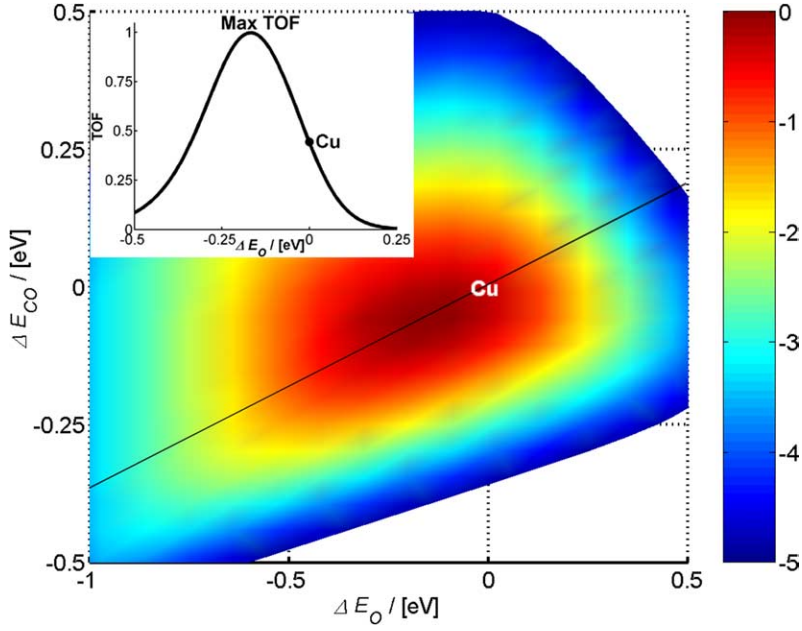

Fig. 8. A close up of the maximum turnover frequency (TOF) at $\xi = 0$, $p = 30$ bar, $T = 225\,^{\circ}\mathrm{C}$, and a feed gas composition of 2.5% CO, 12.5% CO_2, 37.5% H_2, 25%, H_2O, and balance N_2. Based on chemisorption energies from Mavrikakis and co-workers for chemisorption on terrace sites. Insert displays a cut through the maximal TOF and the TOF for Cu.

It is difficult to address whether the WGS reaction occurs on either steps or terraces, or to distinguish between the choice of DFT functionals. In addition, the reaction may be considerably more complex than suggested here. Different steps of the reaction sequence may occur either solely on the terrace or at step sites, thereby involving the participation of two types of sites on the metal particles. In general, we believe that the simple model of the present study captures the essential reactivity trends of the redox mechanism over transition metal catalysts, and it appears to be premature to include effects concerning the influence of surface geometry at this stage.

4.1. Approximations and limitations of the model

To limit the number of variables used to describe the activity trends, it is necessary to make several approxima-

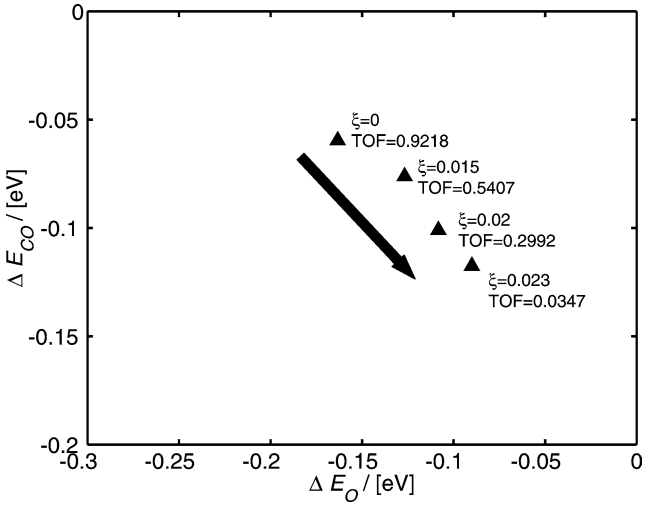

Fig. 9. Coordinates ($\Delta E_{\mathrm{O}}, \Delta E_{\mathrm{CO}}$) for the position of the maximal TOF at different extents of reaction, ξ. $p = 30$ bar, $T = 225\,^{\circ}\mathrm{C}$, and a feed gas composition of 2.5% CO, 12.5% CO_2, 37.5% H_2, 25%, H_2O, and balance N_2. The arrow indicates the shift in optimal adsorption energies, as the reaction progresses. Based on the adsorption energies from [19]. Note that the axes are chosen such that Figs. 9–11 are directly comparable.

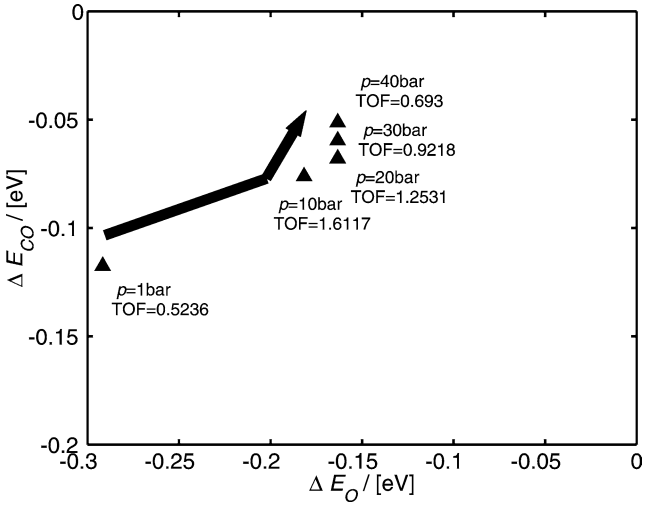

Fig. 10. Coordinates ($\Delta E_{\mathrm{O}}, \Delta E_{\mathrm{CO}}$) for the position of the maximal TOF at different pressures, p. $\xi = 0$ bar, $T = 225\,^{\circ}\mathrm{C}$, and a feed gas composition of 2.5% CO, 12.5% CO_2, 37.5% H_2, 25%, H_2O, and balance N_2. The arrow indicates the shift in optimal adsorption energies, as the pressure rises. Based on the adsorption energies from [19]. Note that the axes are chosen such that Figs. 9–11 are directly comparable.

tions, thereby limiting the validity of the model as one moves away from Cu. We now address the impact of these assumptions.

First of all, we assume that the reaction mechanism is the same on all metals. This may not be justified, since other reaction mechanisms may be suggested for the WGS reaction. Furthermore, the fact that the binding energies are coverage dependent is neglected. This is a particular problem at high coverages, which seems to be the case for the majority of the metals (see Fig. 6). This behavior is the most likely reason

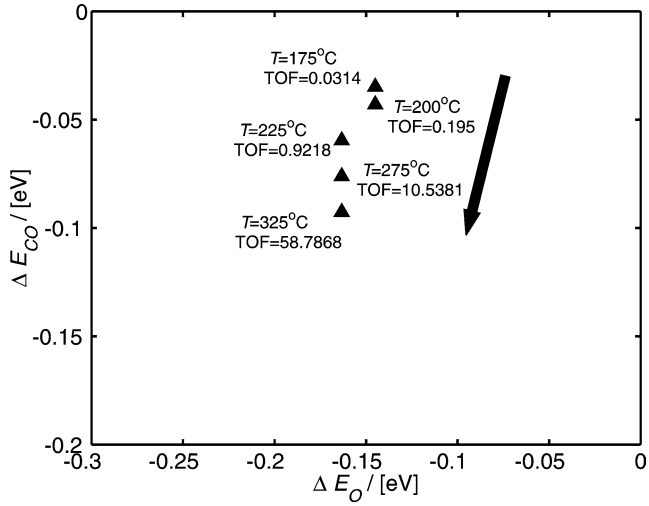

Fig. 11. Coordinates ($\Delta E_{\mathrm{O}}, \Delta E_{\mathrm{CO}}$) for the position of the maximal TOF at different temperatures, T. $\xi = 0$ bar, $p = 30$ bar, and a feed gas composition of 2.5% CO, 12.5% CO_2, 37.5% H_2, 25% H_2O, and balance N_2. The arrow indicates the shift in optimal adsorption energies, as the temperature rises. Based on the adsorption energies from [19]. Note that the axes are chosen such that Figs. 9–11 are directly comparable.

that the model would underestimate the reaction rate for a number of low-activity metals, as discussed later.

Another source of uncertainties is the linear fitting of the chemisorption data (see Tables 1 and 2). Elementary step 7 in particular has large deviation values, and differences between the regression line and the individual data points can be substantial (see Fig. 2a). The result of this is that some of the metal parameters are reproduced quite well, whereas others are far from the linear estimate, leading to deviations in the reaction rate on a number of metals. As long as the model is used only in the vicinity of Cu, the error made in the estimates of the energies will be small, even though there are quite large uncertainties in the slopes, which are used to estimate the energies.

4.2. Improving copper-based WGS catalysts

As a consequence of the aforementioned limitations, the model is most reliable in the parameter space close to Cu. Because there are no other metals in the vicinity of Cu, the most important result of this study is that it gives an idea of what should be done to achieve an improved Cu catalyst. Even though Cu is placed near the maximum of the volcano plot, the WGS reaction rate on a Cu catalyst can be improved, if it is modified to bind both CO and O more strongly to the surface. According to the d-band model developed by Hammer and Nørskov [25], an enhancement of the reactivity of copper may be obtained by growing it as a pseudomorphic layer on top of another metal with a larger lattice constant [26,27]. Here it is important that Cu does not dissolve into the bulk of the host metal, but rather forms islands on the surface of the host metal [28]. It can be questioned whether this approach is favorable, as it is seen in Fig. 5 that the predicted activity can only be improved by a factor of 2. Alloying may

also enhance the activity of the catalyst, but this effect has not been fully clarified in the case of the methanol catalyst, where, for example, Zn may improve the overall rate [29–31]. Improvement in catalyst performance in this case is probably related to the well-known sintering of copper catalysts [2].

4.3. Comparison with experiments/estimated metal rank

When the model is used to estimate the trends in catalytic WGS activity for various transition metals, it is clear that the model is not quantitatively reliable for metals other than Cu. If the predicted rates are compared with the rates measured by Grenoble et al. [32], one finds that, for all metals other than Cu, the predicted rate is several orders of magnitude lower than the measured rate. However, the model reproduces the trends found experimentally by Grenoble et al. [32] surprisingly well. As Grenoble et al. calculated the TOF at conversions below 5%, the best conditions for examining the model estimates should be initial rates for a given gas mixture. Furthermore, the WGS activity was investigated on aluminum oxide support, known to show only weak support effects [32], which is assumed in the model. The order of activity of the transition metals tested for WGS activity at 300 °C and a feed gas containing $p_{CO} = 24.3$ kPa and $p_{H_2O} = 31.4$ kPa was found to be [32]

Cu > Co > Ru > Ni > Pt > Au > Fe > Pd > Rh > Ir.

The estimated WGS activity order under these reaction conditions for transition metals based on chemisorption on step sites [19] is predicted to be

Cu > Co > Ru > Fe > Ni > Rh > Au > Ir > Pd > Pt.

From the chemisorption energies on terraces published by Mavrikakis and co-workers, the order of activity is predicted to be

Cu > Ni > Pt > Rh > Ru > Au > Ir > Pd.

From the chemisorption data of Nørskov and co-workers [19], it is seen that the rates for Fe and Rh are overestimated, the rate over Pt is underestimated, and the rates over the rest of the metals are placed fairly well. When the data from Mavrikakis and co-workers are used, the rate over Rh is overestimated, the rate over Ru is underestimated, but the representation of Pt is good. Iron will most likely be present as an oxide under WGS conditions, which has not been taken into consideration in the present model, and therefore the estimated reaction rate on Fe will be misleading. Regarding Pt, the model predicts that it is essentially WGS inactive, but it is found experimentally to be quite active. This metal seems to be highly poisoned by adsorbed carbon monoxide (see Fig. 6). However, the CO chemisorption energy depends on CO coverage [33,34], and this fact has not been incorporated into the model. As already discussed, a similar coverage effect may also influence a number of other metals, particularly those where the surface coverage is predicted to be close to unity. Because there are no extensive data on this coverage dependence, we have decided not to include it.

Using the data on steps from Nørskov and co-workers [19], we generally obtain a better description of the experimental metal-activity ranking than when we use the data on terraces from Mavrikakis and co-workers. Of course, a complete fit cannot be expected, because other mechanisms may dominate on metals different from copper. For example, spillover of oxygen or hydroxide from the support to the metal particles may also occur, leading to a rate higher than the one estimated here. This is the case, for example, for Au, which becomes a good WGS catalyst when supported on Fe_2O_3, TiO_2, and CeO_2 [35–37]. Finally, there may be undesirable reactions, like the methanation process, which takes place on Ru and Rh [38]. The latter reaction is not a problem for Cu, as it is inactive for methane formation. Nonetheless, it is remarkable that this simplified model can account for so many of the trends.

5. Conclusion

Trends for the catalytic activity of WGS for various transition metals have been studied by estimation of the reaction rate with the use of a microkinetic model where only two descriptors have been used to describe surface reactivity. The model assumes that a simple redox mechanism is dominant over all metal catalysts. Comparing the DFT-derived binding energies for all involved surface intermediates and activation energies for the rate-controlling steps, we found a strong correlation between most of the parameters. Furthermore, by using a Brøndsted–Evans–Polanyi relation, and neglecting any trends in the binding energies of H_2O and CO_2, we reduced the initial ten model parameters to two descriptors, namely the binding energies of carbon monoxide and oxygen. A surprisingly good qualitative estimation of the relative activity order of the different transition metal catalysts was found. However, the model fails to quantitatively reproduce experimental data over such a broad range of metals. This discrepancy can be explained, to some extent, by the fact that the coverage dependence of binding energies has been neglected for most metals in the model. Copper is found to be close to the optimum of the rate calculation, although there is room for improvement. In the vicinity of copper the model is expected to describe the catalyst performance well, and it thus predicts that the activity of the copper-based WGS catalyst could be improved by an increase in the reactivity toward carbon monoxide and oxygen. This conclusion was not obvious prior to the present investigation. Furthermore, our study suggests possible directions for improving the WGS catalyst. We note here that one cannot exclude the possibility that another improved WGS catalyst may be found, which could operate through a reaction mechanism different from the simple redox mechanism used to estimate trends in the present study.

Acknowledgments

We acknowledge the Danish Research Council and the Center of Excellence "Towards a Hydrogen-based Society" (Grants no. 2052-01-0054). Work at the University of Wisconsin-Madison has been partially supported by a DOE-BES Catalysis Science grant (DE-FG-02-03ER15469) and the NSF (CTS-0327959). Computational resources at DOE-NERSC, NPACI, and MSCF-PNNL were utilized for the DFT calculations. We thank Research Scientist C.V. Ovesen from Haldor Topsøe A/S for assistance with her kinetic model.

References

[1] C. Rhodes, G.J. Hutchings, A.M. Ward, Catal. Today 23 (1995) 43–58.
[2] M. Twigg, M. Spencer, Appl. Catal. A 212 (2001) 161–174.
[3] P.B. Rasmussen, P.M. Holmblad, T. Askgaard, C.V. Ovesen, P. Stoltze, J.K. Nørskov, I. Chorkendorff, Catal. Lett. 26 (1994) 373–381.
[4] M. Maack, H. Friis-Jensen, S. Sckerl, J.H. Larsen, I. Chorkendorff, Top. Catal. 22 (2003) 160–161.
[5] Y. Tanaka, T. Utaka, R. Kikuchi, K. Sasaki, K. Eguchi, Appl. Catal. A 242 (2003) 287–295.
[6] H.F. Oetjen, V.M. Schmidt, U. Stimming, F. Trila, J. Electrochem. Soc. 143 (1996) 3838–3842.
[7] S. Dahl, J. Sehested, C.J.H. Jacobsen, E. Törnqvist, I. Chorkendorff, J. Catal. 192 (2000) 391–399.
[8] C.J.H. Jacobsen, S. Dahl, A. Boisen, B.S. Clausen, H. Topsøe, A. Logadottir, J.K. Nørskov, J. Catal. 205 (2002) 382–387.
[9] K. Klier, Adv. Catal. 31 (1982) 243–313.
[10] C.T. Campbell, K.A. Daube, J. Catal. 104 (1987) 109–119.
[11] C.T. Campbell, B.E. Koel, K.A. Daube, J. Vac. Sci. Technol. A 5 (1987) 810–813.
[12] J. Nakamura, J.M. Campbell, C.T. Campbell, J. Chem. Soc., Faraday Trans. 86 (1990) 2725–2734.
[13] C.V. Ovesen, Kinetic Modeling of Reactions on Cu Surfaces, PhD Thesis, DTU, (1992).
[14] C.V. Ovesen, P. Stoltze, J.K. Nørskov, C.T. Campbell, J. Catal. 134 (1992) 445–468.
[15] C.V. Ovesen, B.S. Clausen, B.S. Hammershøi, G. Steffensen, T. Askgaard, I. Chorkendorff, J.K. Nørskov, P.B. Rasmussen, P. Stoltze, P. Taylor, J. Catal. 158 (1996) 170–180.
[16] C.V. Ovesen, B.S. Clausen, J. Schiøtz, P. Stoltze, H. Topsøe, J.K. Nørskov, J. Catal. 168 (1997) 133–142.
[17] T. Bligaard, K. Honkala, A. Logadottir, J.K. Nørskov, S. Dahl, C.J.H. Jacobsen, J. Phys. Chem. B 107 (2003) 9325–9331.
[18] J. Greeley, J.K. Nørskov, M. Mavrikakis, Ann. Rev. Phys. Chem. 53 (2002) 319–348.
[19] T. Bligaard, J.K. Nørskov, S. Dahl, J. Matthiesen, C.H. Christensen, J. Sehested, J. Catal. 224 (2004) 206–217.
[20] J.K. Nørskov, T. Bligaard, A. Logadottir, S. Bahn, L.B. Hansen, M. Bollinger, H. Bengaard, B. Hammer, Z. Sljivancanin, M. Mavrikakis, Y. Xu, S. Dahl, C.J.H. Jacobsen, J. Catal. 209 (2002) 275–278.
[21] V. Pallassana, M. Neurock, J. Catal. 191 (2000) 301–317.
[22] P.A. Thiel, T.E. Madey, Surf. Sci. Rep. 7 (1987) 211–385.
[23] P.B. Rasmussen, P.A. Taylor, I. Chorkendorff, Surf. Sci. 269/270 (1992) 352–359.
[24] N. Lopez, J.K. Nørskov, J. Am. Chem. Soc. 124 (2002) 11262–11263.
[25] B. Hammer, J.K. Nørskov, Adv. Catal. 45 (2000) 71–129.
[26] M. Mavrikakis, B. Hammer, J.K. Nørskov, Phys. Rev. Lett. 81 (1998) 2819–2822.
[27] Y. Xu, M. Mavrikakis, Surf. Sci. 494 (2001) 131–144.
[28] A. Christensen, A.V. Ruban, P. Stoltze, K.W. Jacobsen, H.L. Skriver, J.K. Nørskov, F. Besenbacher, Phys. Rev. B 56 (1997) 5822–5834.
[29] N.-Y. Topsøe, H. Topsøe, Top. Catal. 8 (1999) 267–270.
[30] J. Nakamura, I. Nakamura, T. Uchijima, Y. Kanai, T. Watanabe, M. Saito, T. Fujitani, J. Catal. 160 (1996) 65–75.
[31] J. Greeley, A.A. Gokhale, J. Kreuser, J.A. Dumesic, H. Topsøe, N.-Y. Topsøe, M. Mavrikakis, J. Catal. 213 (2003) 63–72.
[32] D.C. Grenoble, M.M. Estadt, D.F. Ollis, J. Catal. 67 (1981) 90–102.
[33] E.K. Vestergaard, P. Thostrup, T. An, E. Lægsgaard, I. Stensgaard, B. Hammer, F. Besenbacher, Phys. Rev. Lett. 88 (2002) 259601.
[34] J.C. Davies, R.M. Nielsen, L.B. Thomsen, I. Chorkendorff, Á. Logadóttir, Z. Łodziana, J.K. Nørskov, W. Li, B. Hammer, S.R. Longwitz, J. Schnadt, E.K. Vestergaard, R.T. Vang, F. Besenbacher, Fuel Cells (2004), accepted for press.
[35] D. Andreeva, V. Idakiev, T. Tabakova, A. Andreev, J. Catal 158 (1996) 354–355.
[36] F. Boccuzzi, A. Chiorino, M. Manzoli, D. Andreeva, T. Tabakova, L. Ilieva, V. Iadakiev, Catal. Today 75 (2002) 169–175.
[37] Q. Fu, S. Kudriavtseva, H. Saltsburg, M. Flytzani-Stephanopoulos, Chem. Eng. J. 93 (2003) 41–53.
[38] T. Utaka, T. Okanishi, T. Takeguchi, R. Kikuchi, K. Eguchi, Appl. Catal. A 245 (2003) 343–351.